Arabian Journal of Geosciences (2024) 17:124
https://doi.org/10.1007/s12517-024-11916-5

ORIGINAL PAPER

Petrology of volcano-sedimentary deposits from Mayo Mbota, west of the Cretaceous Babouri-Figuil basin, North Cameroon

Tchomsinba Il Lévis[1] · Augustin Désiré Balla Ondoa[1] · Lise Carole Okomo Atouba[2] · Fagny Mefire Aminatou[1] · Faarouck Oumarou Nkouandou[1]

Received: 2 November 2023 / Accepted: 25 February 2024 / Published online: 14 March 2024

Abstract

The investigation of volcano-sedimentary rocks situated to the west of the Cretaceous Babouri-Figuil basin involved a comprehensive characterization encompassing petrography, mineralogy, and geochemistry. The sedimentary formations were classified into four distinct facies: coarse sandstones, medium sandstones, fine sandstones, and schistose marls. Additionally, post-sedimentary lava flows composed of andesitic basalts were identified. Petrographic analysis revealed quartz as the predominant constituent in the sedimentary rocks. The volcanic rocks exhibited two distinct textures: a microlitic porphyritic texture, featuring oxides, plagioclase phenocrysts, and clinopyroxenes, and a doleritic porphyritic texture, wherein the rock volume comprised 10–15% automorphic plagioclase phenocrysts (1 to 3.6 mm), 20% clinopyroxenes (1.5 mm), 2–7% oxide crystals (less than 1 mm), 2% olivines, and approximately 1% amphibole phenocrysts (> 1 mm). The identified mineral phases were categorized into two groups: primary minerals (calcite, feldspar, quartz, muscovite) and secondary minerals (kaolinite, illite, smectite), along with titanium oxides, anatase, hydrated sodium silicates, and analcime. Geochemical analysis of the basalts indicated their classification as oceanic tholeiites, suggesting a composition of andesitic basalts emplaced within an orogenic setting. The Mayo Mbota sediments were categorized as intermediate to acidic rocks associated with active continental margins, deposited in an arid to semi-arid environment. These sediments were derived from the accumulation of alteration products of felsic rocks.

Keywords Petrography · Mineralogy · Geochemistry · Volcano-sedimentary · Mayo Mbota · Babouri-Figuil basin

Introduction

The Babouri-Figuil basin, situated in Cameroon, is an intracontinental basin. The establishment of the South Atlantic Ocean, initiated by the dislocation of Gondwana in the Valanginian (Sibuet and Mascle 1978), led to the subsidence of the Benue Gap. The Cretaceous Babouri-Figuil basin, an extension of the Yola branch (Fig. 1(b)), emerged as one of several small basins during this period. Geological processes, including plutonism, metamorphism, sedimentation, and volcanism, have significantly impacted the North-South axis of the Western sector of the Babouri-Figuil basin.

The central part of the basin, particularly in the locality of Babouri, experienced multiple episodes (3) of lava flows, forming a distinctive block structure. Subsequent extensive and centripetal alteration occurred in onion skins (Balla 2017). These lava flows have both calcined and metamorphosed various sedimentary deposits, notably schistose marls, as they traversed them. The sedimentary series can reach a thickness of up to 1500 m (Schwoerer 1965). The basin drains westward through tributaries of the Mayo Oulo (Fig. 1(c)), with the main seasonal tributary being the Mayo Mbota.

The Mayo Mbota region exhibits basaltic flows interstratified within clayey sediments, constituting a geological activity with poorly understood characteristics. This activity may result in contamination between different rock types during emplacement or the transfer of elements. The objective

Responsible editor: Attila Ciner

✉ Augustin Désiré Balla Ondoa
auguste1balla@gmail.com

[1] Department of Earth Sciences, Faculty of Science, University of Ngaoundere, P.O. Box 456, Ngaoundere, Cameroon

[2] Higher Teacher Training College, University of Bertoua, P.O. Box 652, Bertoua, Cameroon

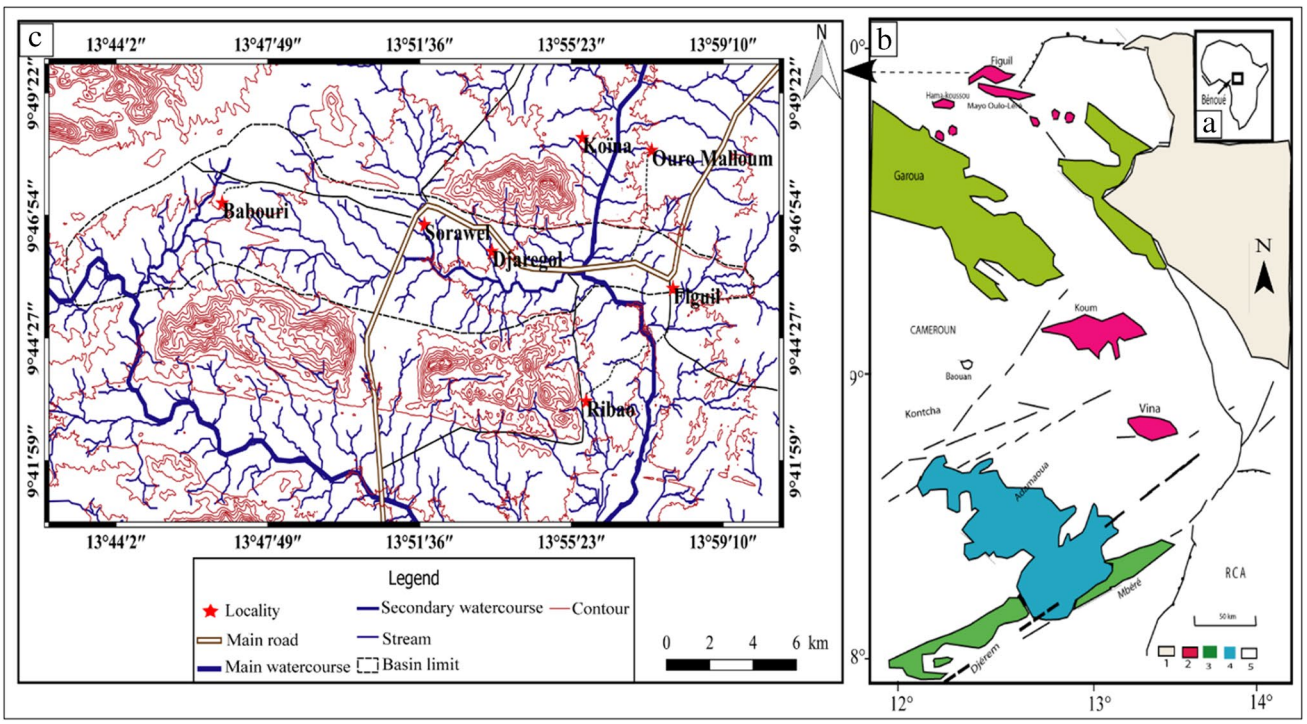

Fig. 1 (**a**) Map of Africa. (**b**) Location map of the sedimentary basins of northern Cameroon (modified after Maurin and Guiraud 1990). 1, terminal continental; 2, Barremo-Aptian basins; 3, Albo-Aptian to Cenomanian-Turonian basins; 4, volcanism; C, map of the Babouri-Figuil basin (satellite image)

of this study is to conduct a comprehensive petrographical, mineralogical, and geochemical characterization of the oceanic tholeiites and schistose marls in the Mayo Mbota region of the Babouri-Figuil basin.

Geological context

The Pan-African chain in Cameroon is part of the Central African Orogenic Belt, constituting a mega-chain oriented in an east-west direction, spanning over 5000 km in length and 3000 km in width. Bounded to the west by the Pan-African Trans-Saharan Range and to the south by the Congo Craton, it extends northeast into Brazil as the Neoproterozoic Sergipano Range, collectively forming the Pan-African-Brazilian Range (Almeida et al. 1981; Davison and Reginaldo 1989; Castaing et al. 1993; Brito de Neves et al. 2001).

The significant characteristics of the North Equatorial Pan-African Range in Cameroon have been elucidated in various works by Nzenti et al. (1992, 1994, 1998), Ngnotué et al. (2000), Toteu et al. (2004), and Tanko Njiosseu et al. (2005). In Cameroon, the North Equatorial Pan-African Range comprises three distinct geodynamic domains (Fig. 2): (1) a southern domain, (2) a central domain, and (3) a northern domain, which will be described herein.

The North Cameroon domain extends from the south of Poli to the northern tip of Cameroon. It is characterized by a polyphase and polycyclic evolution (Toteu et al. 1987; Nzenti et al. 1992; Ngako 1999), marked by three phases of deformation staggered from D1 to D3. The first phase, D1, early and tangential (800–700 Ma, U/Pb age on zircon, Toteu et al. 1990), is associated with structures often obliterated by subsequent phases D2 and D3. The Neoproterozoic age metamorphism linked to this D1 phase exhibits amphibolite facies assemblages (650 °C, 6–7 Kb, Nzenti et al. 1992) represented by Crd + Grt + Sill + Qtz + Kfs + Pl and Hbl + Grt + Pl + Qtz.

The second phase, D2, is synchronous with intense magmatism (Njel 1988; Nzenti et al. 1992) and granitization (D2 syntectonic calc-alkaline granitoids dated at 580 Ma, U/Pb age on zircon, Toteu et al. 1987). D2 is associated with N-S or NW-SE sinistral rifts, thrusting, and E-W to WSW-ENE echelon antiforms and synforms. Amphibolite (700 °C, 5–7 Kb) and greenschist (550 °C, 5 Kb) facies metamorphism are related to this phase, exhibiting mineralogical assemblages such as Qtz + Pl + Hbl + Bt + Spn + Ilm + Epi and Qtz + Pl + Bt + Spn + Ms + Grt (amphibolite facies), as well as Qtz + Alb + Ch + Ms + Cc and Qtz + Pl + Ms + Bt + Grt + St (greenschist facies).

The third deformation phase, D3, is brittle and gives rise to numerous E-W dextral rifts and E-W and N-S trending

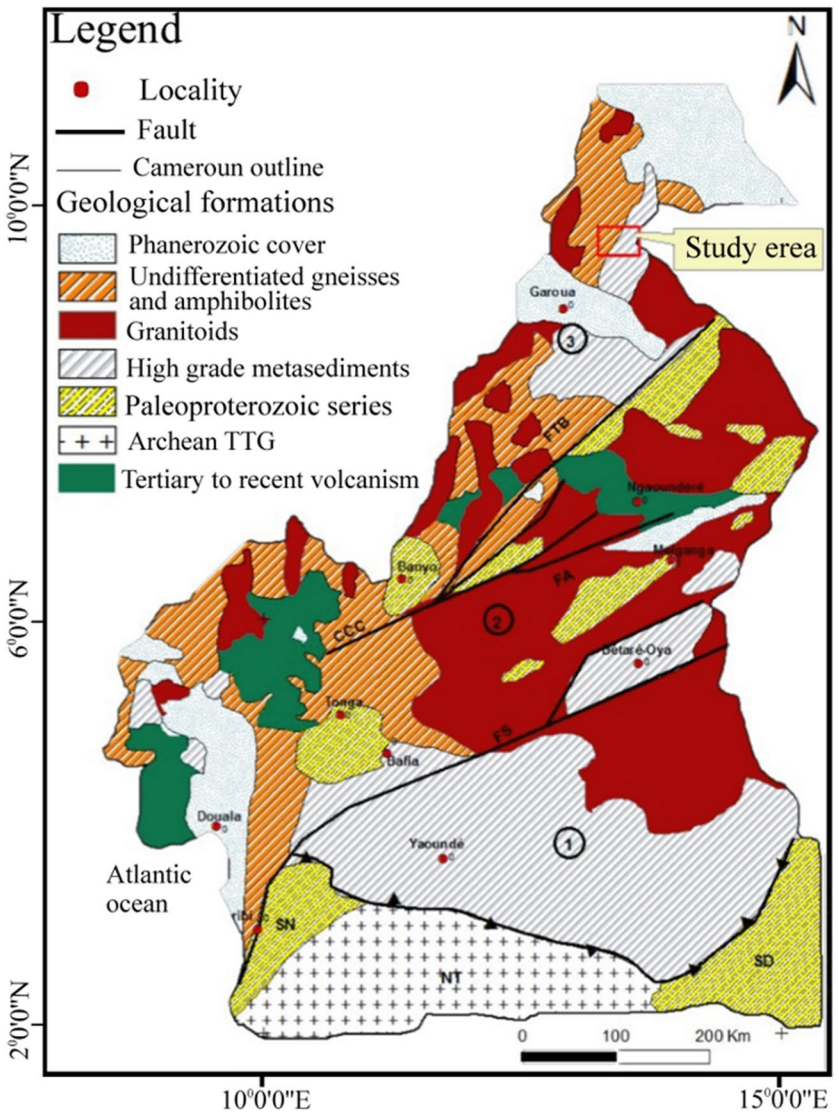

Fig. 2 Geological map of Cameroon (Nzenti et al. 2011) showing the location of the Nola Mbétem-Viali sector and the main lithotectonic domains: (1) southern domain; (2) central domain; (3) northern domain; CCC, Cameroon Central Shear; FS, Sanaga Fault; FTB, Tibati-Banyo Fault; NT, Ntem complex; SD, Dja series; SN, Nyong series; FA, Adamaoua Fault

folds. Syn-D3 granitoids, dated at 545 Ma (U/Pb age on zircon, Toteu et al. 1987), have also been observed.

Materials and methods

The sedimentological investigation of this section of the basin was conducted in a north-south direction to elucidate the spatio-temporal relationships among the layers. This approach resulted in the construction of a lithological log. A total of 15 samples were collected: 5 samples of volcanic rock and 10 samples of sedimentary rock, intended for thin section, geochemical, and mineralogical analyses. Sample preparation was carried out at the Geochemical Mapping and Metallogeny Laboratory of the University of Ngaoundere.

Subsequently, mineralogical analyses were performed at the Geoscience Laboratories in Ontario, Canada (Geo Labs), utilizing Co-DRX at 40 KV and 45 Ma on the samples. Geochemical analyses were conducted at Bureau Veritas Commodities Laboratory, Vancouver, Canada, using ICP-AES (for major elements) and ICP-MS (for trace elements) after fusion with $LiBO_2$. The sample processing involved the use of a jaw crusher with steel plates, followed by pulverization in a ball mill. The fraction below 100 µm was utilized for analysis.

X-ray diffraction (XRD-100) was employed for mineralogical analysis, involving the pulverization of sample powders with an agate mortar and pestle, and smear mounts were prepared on low background silicon discs for analysis. The Co radiation at 40 kV and 45 mA was utilized for the analysis, employing the X'Pert HighScore software. This software operates on the principle that the distances between successive atomic planes (d) are specific to each mineral, producing a refraction signal at an angle 2θ represented as a peak relative to the flat surface of the mineral. The angle allows the calculation of the corresponding value (d) through

Bragg's law, based on which the standard conversion tables of the U.S. Geological Survey were defined: $n\lambda = 2d \sin \theta$, with n as the diffraction order, λ as the wavelength of the radiation used in Å, d as the lattice space, and θ as the angle of incidence.

Wavelength dispersive X-ray fluorescence spectrometry (WD-XRF) was employed for major element determination. This analytical procedure was complemented by the use of the ICP-AES methodology (model IAT-100). Calibration maintenance, review of calibration robustness, and verification of lower detection limits (LLDs) were conducted to ensure the high quality of routine analyses. The determination of trace elements using the Perkin Elmer Elan 9000 method achieved increased precision and accuracy above 10% for most elements. The laboratory monitors the performance of each method through inter-laboratory and in-house reference material analysis control charts, and the overall accuracy of analytical methods is assessed from the reproducibility of analyses of reference materials reviewed as quality assurance monitors during the analytical process.

Results

Lithology and sedimentology

Volcanic activity has been observed in the vicinity of the Mayo Mbota River, where three distinct volcanic episodes have been identified along the river course. The sedimentary lithology within this segment of the basin displays a vertical sequence as follows, from the base to the summit: a robust layer of ferruginized, non-calcitic, and highly compact coarse sandstone, succeeded by a fine, ferruginous, and exceptionally hard sandstone. Subsequently, there is coarse sandstone featuring N-W trending diaclases, followed by a substantial layer of medium-pink sandstone, a layer of fine sandstone, and another layer of coarse ferruginous sandstone.

Continuing upwards, the lithological sequence comprises a substantial layer of shale marl, followed by a siltstone layer and another layer of shale marl. This is succeeded by a medium sandstone layer, a layer of fine sandstone, and another layer of shale marl. Further up, there is a layer of coarse sandstone exhibiting ripple marks, indicative of the basin's northward feeding, overhung by fine sandstone, medium sandstone, and fine. The sequence concludes with layers of shale marlstone, medium sandstone, shale marlstone, a volcanic intrusion, shale marlstone, medium sandstone, another volcanic intrusion, shale marlstone, and a final volcanic intrusion.

The litho-stratigraphic synthesis of this basin segment is visually represented in Fig. 3, illustrating eight depositional

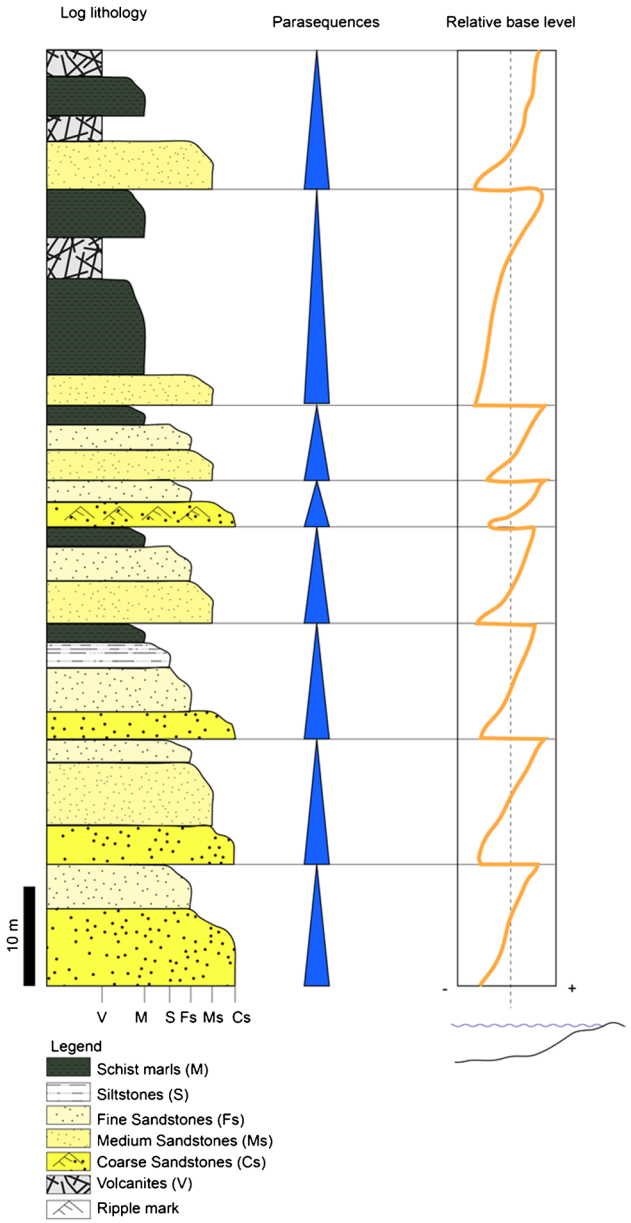

Fig. 3 Synthetic litho-stratigraphic log of the Mayo Mbota outcrop

parasequences that collectively depict a monotonic sedimentation pattern.

Petrographic study

Petrography of sedimentary rocks

The analysis of thin slides from sandstone rocks in the western part of the Babouri-Figuil basin indicates that quartz is the predominant mineral in both coarse and fine sandstones. Quartz grains occasionally exhibit cracks (Fig. 4C) and a crumpled appearance. Feldspars present a cloudy appearance, suggesting significant chemical alteration. Mottled

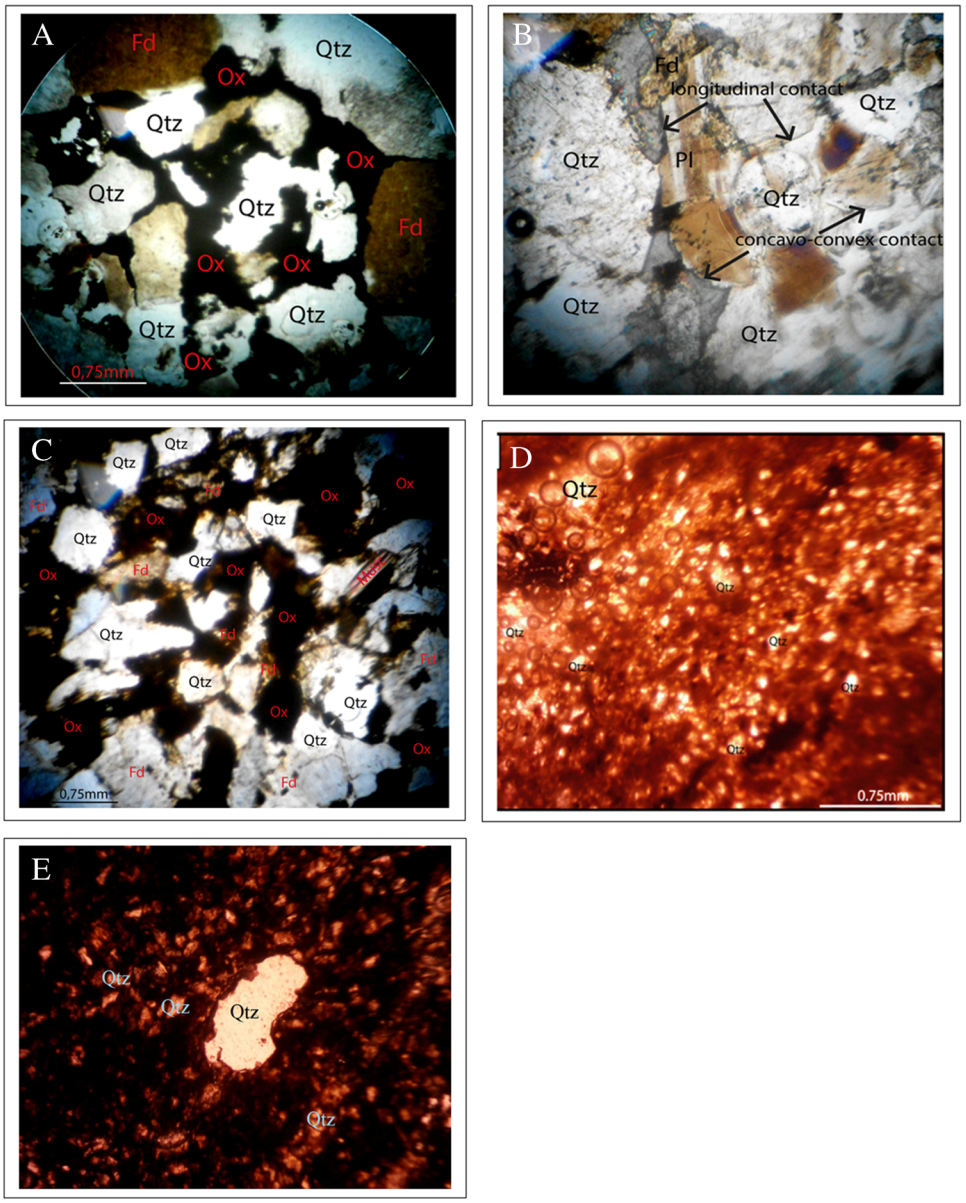

Fig. 4 **A**–**C** Polarizing microscopic aspects of thin sections of sandstone rocks in the western part of the basin. **A** Altered feldspars in coarse sandstone with abundant oxides in a ferruginous cement. **B** Large plagioclase pebbles in a fine sandstone on quartz minerals that show tangential contacts. **C** Coarse sandstone with muscovite flakes and much iron cement. **D** Thin sheet of unmetamorphosed marl showing quartz microcrystals. **E** Thin sheet of metamorphosed marl

plagioclases are observable in the fine sandstone (Fig. 4B). Amphiboles appear greenish in unpolarized light (LPNA) and show slight color variation in polarized light analysis (LPA). Mica flakes are dispersed among the quartz grains (Fig. 4C). These features are overlaid by a siliceous clay matrix mixed with iron oxides (Fig. 4A, C).

The petrographic examination of Mayo Mbota sediments in the Babouri-Figuil basin reveals diverse contacts between grains, ranging from tangential (Fig. 4A, C) and frank contacts to concavo-convex and longitudinal contacts. The concavo-convex contacts (Fig. 4B) exhibit hollows on their surfaces corresponding to impressions of neighboring particles, indicative of extensive mechanical compaction.

Schistose marls exhibit three aspects: weakly metamorphosed to metamorphosed or not metamorphosed, depending on the heat introduced by basaltic flows. Unmetamorphosed marls are greenish with a brown matrix and very small quartz crystals (Fig. 4D). Weakly metamorphosed and fully metamorphosed marlstones are respectively grey, dark, and black with a black matrix (Fig. 4E). They all display a pisolitic to oolitic texture. The matrix reveals (1) quartz crystals with an increasingly cloudy appearance in the metamorphosed marlstones and (2) agglomerations of oolites, geological concretions of small, regular, spherical mineral structures similar to fish eggs.

Petrography of volcanic rock

The volcanic prisms forming the eruptive episodes exhibit a centrifugal alteration, visually represented by an onion

skin structure (Fig. 5A, B). The marlstones are entirely altered below these volcanic flows. In the majority of instances, the volcanic deposits display veins filled with late calcite, which appears to be younger compared to those observed in fine sandstones and coarse sandstone layers, where they exhibit a sinister dip (Balla et al. 2022). It could be hypothesized that volcanism serves as the source of the calcite present in the diaclase veins.

The basalts outcrop in centimetric balls between the clayey sediments. They present two textures: a microlitic texture (Fig. 6A, B) which shows, in addition to oxides, elongated plagioclase phenocrysts, the largest of which is rectangular in shape and is in the process of being altered (Fig. 6B), and clinopyroxenes, a doleritic porphyritic texture (Fig. 6C, F) with 10–15% of the rock volume containing automorphic plagioclase phenocrysts (1–3.6 mm), 20 w.% clynopiroxenes (1.5 mm), 2–7 w.% oxide crystals (smaller than 1 mm), 2% olivine, and amphibole phenocrysts (> 1 mm) about 1% of the rock volume.

Mineralogy

Analysis of the diffractograms facilitated the identification of nine mineral phases, which were categorized into two groups (Fig. 7). The primary minerals, including calcite, feldspar, quartz, and muscovite, were the most abundantly represented. Secondary minerals, such as kaolinite, illite, and smectite, were also observed. Additionally, titanium oxides like anatase and hydrated sodium silicates such as analcime were identified.

Geochemistry

The chemical compositions of representative samples of basalts and marls are shown in the table below.

Geochemistry of basalts

The basalts exhibit intermediate silica contents ranging from 52.0 to 52.6 w.% and low alkali contents ($Na_2O + K_2O <$ 3.3 w.%) (Table 1). Based on the volcanic rock nomenclature proposed by Le Maître (2002), the composition of these basalts falls within the range from andesitic basalts to Babouri basalts (Fig. 8). The MgO and Fe_2O_3 concentrations are between 7.04 and 7.29 w.% and 11.4 and 12.3 w.%, respectively. The Mg number (Mg#) calculated using these values ranges from 51.36 to 52.39 w.% (Table 1). The basalts are characterized by TiO_2 contents between 1.92 and 2.07 w.% and low K_2O and P_2O_5 contents. The concentrations of MgO and Fe_2O_3 categorize the basalts as tholeiites (Fig. 9A), specifically falling into the oceanic types on the triangular diagram (TiO_2–P_2O_5–K_2O) of Pearce (1975) (Fig. 9B).

Transition elements Cr and V exhibit high contents (250–300 ppm and 183–211 ppm). Alkaline (Rb 8.7–10.6 ppm) and alkaline earth elements (Ba 126.5–151 ppm and Sr 281–297 ppm) are relatively high (Table 2) compared to the early mantle ratio of McDonough and Sun (1995). Elements such as U, Y, Th, and Zr have concentrations between 0.26 and 0.3 ppm, 22.1 and 22.3 ppm, 0.97 and 1.01 ppm, and 115 and 126 ppm, respectively.

The normalized multi-element spectra of the tholeiitic basalts exhibit a very shallow slope with weak positive anomalies in Ba and Sr and negative anomalies in Th, U, P, and Ti (Fig. 10). These spectra closely resemble those of the tholeiites in the Mayo Oulo basin (Ngounouno et al. 2001). The rare earth spectra show a negative slope from La to Lu with almost no anomaly (Table 3), (Fig. 11).

The geodynamic context of the Baburi tholeiitic basalts is discerned through triangular diagrams constructed from immobile trace elements. In the triangular diagram (Y/15-La/10-Nb/8) of Cabanis and Lecolle (1988), the Baburi tholeiitic basalts are situated at the boundary of the late to post-orogenic (compressive to distensive) intracontinental

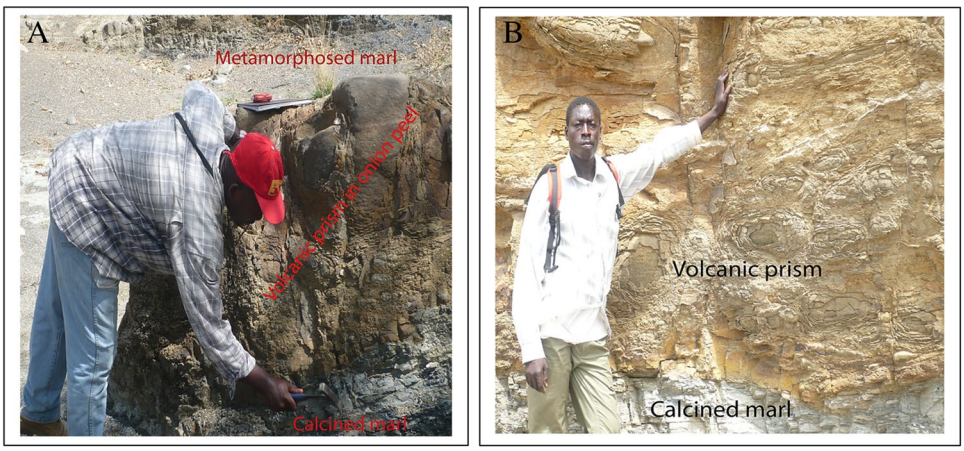

Fig. 5 Volcanic flows. **A** Metamorphosed marlstones below the flows; **B** volcanic prism showing onion skin alteration

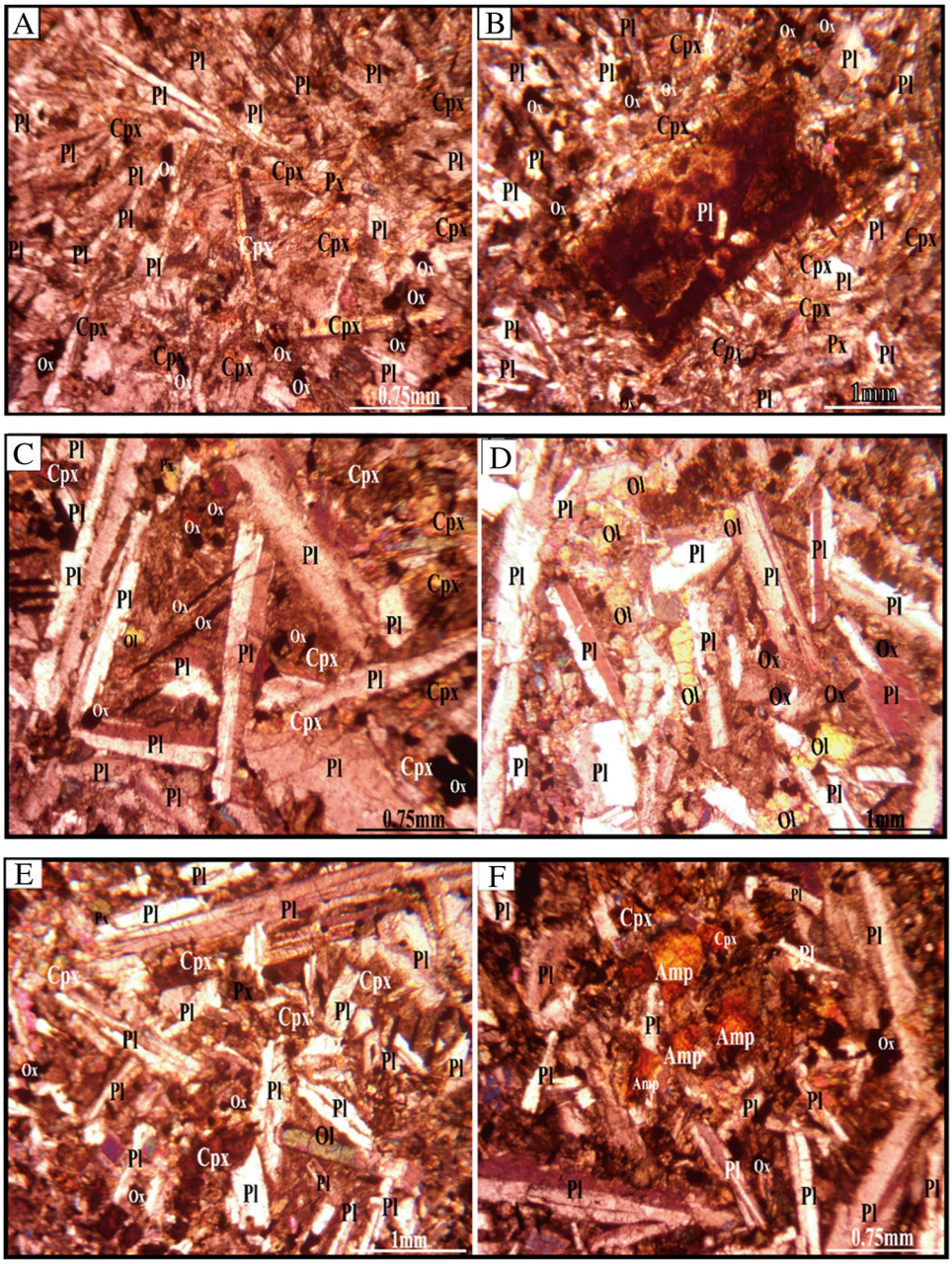

Fig. 6 Thin basalt sheet with porphyry microlitic and doleritic texture. **A** Elongated plagioclase and clinopyroxene crystals; **B** rectangular plagioclase crystals undergoing alteration. **C** Association of Pl-Cpx-Ox. **D** Cracked Ol in net contact with Pl. **E** Olivine in gross contact with Pl. **F** Amphibole in association with some clinopyroxenes and plagioclases

domains and the non-orogenic (distensive) domains (Fig. 12A). In the triangular diagram (Th-3Tb-2Ta) of Cabanis and Thiéblemont (1989), the Baburi tholeiitic basalts are predominantly located in the anorogenic domain of ridge tholeiites and intraplate alkaline basalts (Fig. 12B).

Geochemistry of the marls

The major elements present in the Babouri marls include SiO_2, Al_2O_3, Fe_2O_3, and CaO, with ranges of 28.58–61.79 w.%, 7.87–16.8 w.%, 2.99–9.78 w.%, and 1.65–17.66 w.%, respectively. Less abundant elements such as MgO, K_2O, Na_2O, and TiO_2 and trace elements like MnO and P_2O_5 are also identified (Table 1). The SiO_2/Al_2O_3 ratio in the Babouri marls ranges from 3.12 to 4.12 w.% (Table 1). Using the diagram defined by Suttner and Dutta (1986), the sedimentary environment and chemical maturity of the marls suggest deposition in an arid to semi-arid environment with a moderate degree of chemical maturity (Fig. 13).

The Chemical Alteration Index (CIA), which measures the degree of chemical alteration according to Young and Nesbitt (1998), is calculated using the formula CIA = $[Al_2O_3/(Al_2O_3 + K_2O + Na_2O + CaO) * 100]$. The CIA values for the Babouri marls range from 17.21 to 64.31 w.%, indicating a positive correlation between TiO_2 and Al_2O_3.

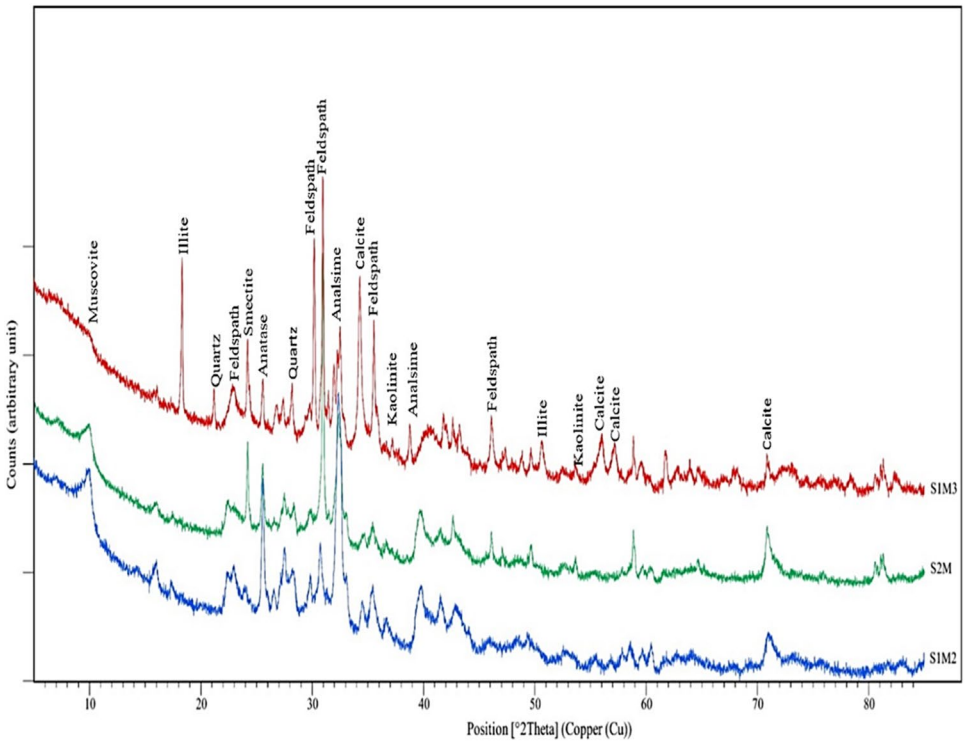

Fig. 7 Mineral phases of the Mayo Mbota marls

Table 1 Major elements (w.%) of Mayo Mbota marl and basalt and ratio of certain elements

	S1M3	S2M2	S1M4	S2M1	S3M5	S1Vol1	S1Vol2	S2Vol3
SiO_2	47.00	52.50	52.86	28.50	61.79	52.60	52.00	52.60
Al_2O_3	13.85	16.80	12.99	7.91	14.99	13.45	13.10	13.60
Fe_2O_3	6.89	9.78	4.20	5.56	2.99	12.30	11.90	11.40
CaO	7.11	1.65	10.21	17.66	5.04	8.73	8.60	8.67
MgO	2.86	5.16	1.94	9.43	2.53	7.29	7.12	7.04
Na_2O	2.85	1.83	5.20	2.78	5.85	2.65	2.58	2.66
K_2O	2.86	3.07	1.21	1.25	1.35	0.44	0.40	0.53
TiO_2	1.12	0.90	0.44	0.36	0.62	2.07	2.02	1.92
MnO	0.10	0.08	0.14	0.15	0.07	0.16	0.15	0.14
P_2O_5	0.21	0.17	0.14	0.10	0.17	0.21	0.23	0.20
LOI	13.50	9.35	10.50	25.80	4.50	1.76	1.89	2.27
sum	98.35	101.29	99.83	99.50	99.90	101.66	99.99	101.03
k_2O/Na_2O	1.00	1.67	0.23	0.45	0.23	0.17	0.16	0.20
SiO_2/Al_2O_3	3.39	3.13	4.07	3.60	4.12	3.91	3.97	3.87
Na_2o+K_2O	5.71	4.90	6.41	4.03	7.20	3.09	2.98	3.19
SiO_2/Al_2O_3	3.39	3.12	4.06	3.60	4.12	3.91	3.97	3.88
CIA	40.07	64.31	31.37	17.21	43.34			
Mg#						51.36	51.60	52.39

CIA (%) = $[Al_2O_3/(Al_2O_3 + CaO^* + Na_2O + K_2O)] \times 100$. Mg# = 100*(MgO/40.32)/((MgO/40.32)+(FeOt/71.85)

Characterization of the source of the marls

The origin of the Babouri marls is attributed to the accumulation of alteration products derived from rocks with acid to intermediate characteristics (Fig. 14A), as indicated by the diagram defined by Floyd et al. (1990). Additionally, these marls fall within the wacke field (Fig. 14B) according to Herron (1988).

Alkalis such as Rb exhibit values ranging from 20.4 to 104 ppm. Alkaline earth elements such as Ba and Sr

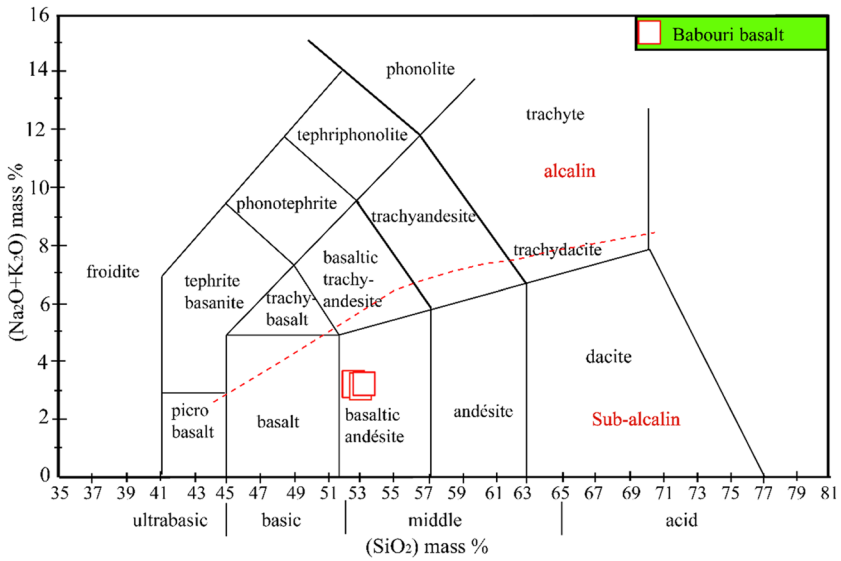

Fig. 8 Nomenclature of the Babouri basalts according to the TAS diagram (Le Maître 2002). The dashed red line represents the boundary between the alkaline and sub-alkaline domains

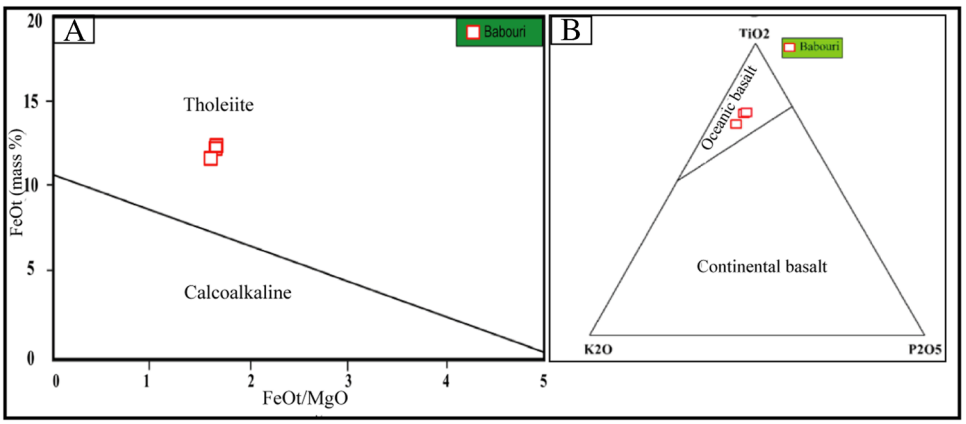

Fig. 9 Situation of the Babouri basalts: **A** in the FeOt = f(FeOt/MgO) diagram of Miyashiro (1974), **B** in the triangular diagram TiO_2–K_2O–P_2O_5 of Pearce (1975)

have concentrations between 506 and 641 ppm and 250.8 and 1790 ppm, respectively. The trace element spectrum (Fig. 15), normalized to the North American shale composite (NASC) standard (Gromet et al. 1984), reveals variations in the concentrations (peak intensities) of elements, with negative anomalies in Th, U, and Hf. Non-metamorphosed samples (S1M3, S1M4, and S3M5) show a positive Sr anomaly. The Th/U, Zr/Y, and Hf/Ta ratios have values below 1 w.%.

The most abundant rare earth elements are Ce (30.8 ppm and 117.5 ppm), La (16.9 ppm and 56.1 ppm), and Nd (13.4–52.1 ppm). The chondrite-normalized rare earth concentration curves (Gromet et al. 1984) display a negatively sloping curve from La to Lu with a negative anomaly in Eu (Fig. 16). In interpreting the rare earth element distribution, the chondrite-normalized spectrum (Pourmand et al. 2012) indicates a high concentration of light rare earth elements (LREEs) and a depletion of heavy rare earth elements (HREEs). A nearly flat spectrum of heavy rare earths ranging from gadolinium to lutetium is observed (Fig. 16). In other words, heavy rare earths and light rare earths exhibit differential mobility in a supergene environment. The high rare earth fractionation with an increasing (La/Yb)N ratio is directly proportional to the increase in alteration degree (Ma et al. 2007; Yusoff et al. 2013).

Discussion

The interbedded arrangement of tholeiitic basaltic rocks and marly sedimentary rocks suggests (1) a common age of emplacement for these formations and (2) a basin emplacement pattern that commenced with subsidence, followed by sedimentary infilling and, subsequently, repeated volcanic eruptions.

The contact between basaltic and sedimentary formations led to varying degrees of metamorphism in the sedimentary rocks. This diversity can be attributed to temperature

Table 2 Trace elements (ppm) in sedimentary and volcanic rocks of Mayo Mbota

	S1M3	S2M2	S1M4	S2M1	S3M5	S1Vol1	S1Vol2	S2Vol3
Ba	641.00	506.00	550.00	517.00	351.00	131.50	126.50	151.00
Ce	117.50	102.50	30.80	62.50	38.40	23.20	22.50	21.20
Cr	70.00	90.00	27.36	27.36	44.00	280.00	300.00	250.00
Cs	2.22	1.75	0.40	0.60	0.50	0.10	0.02	0.14
Dy	7.69	6.85	2.76	5.17	5.15	5.03	4.83	4.60
Er	4.21	3.58	1.68	3.33	3.36	2.45	2.64	2.20
Eu	1.98	1.78	0.77	1.22	1.20	1.64	1.77	1.55
Ga	23.70	26.90	13.50	8.80	13.50	21.20	21.50	20.40
Gd	8.94	7.92	2.93	5.27	4.85	5.31	5.17	4.90
Hf	6.20	6.10	3.20	2.10	5.30	3.40	3.80	3.30
Ho	1.33	1.15	0.57	1.07	1.14	0.80	0.86	0.80
La	56.10	50.50	16.90	28.90	17.70	10.00	9.70	9.20
Lu	0.47	0.46	0.23	0.45	0.47	0.28	0.25	0.26
Nb	25.10	25.60	4.50	4.00	6.50	10.90	11.00	9.60
Nd	52.10	44.50	13.40	27.90	17.70	15.10	15.00	14.30
Pr	13.55	11.80	3.40	14.47	4.48	3.30	3.15	2.76
Rb	104.00	90.40	20.40	26.70	25.40	9.30	8.70	10.60
Sm	10.50	9.04	2.58	5.24	3.99	4.59	4.62	3.95
Sn	4.00	3.00	1.00	1.00	1.00	1.00	1.00	1.00
Sr	588.00	265.00	576.20	179.04	250.80	292.00	297.00	281.00
Ta	1.60	1.80	0.30	0.20	0.40	0.70	0.70	0.60
Tb	1.30	1.15	0.43	0.85	0.79	0.84	0.74	0.78
Th	15.75	11.95	2.10	8.40	3.20	1.01	0.99	0.97
Tm	0.57	0.48	0.24	0.50	0.41	0.25	0.28	0.25
U	1.60	2.02	0.30	0.50	0.30	0.30	0.26	0.26
V	101.00	148.00	51.00	57.00	60.00	194.00	211.00	183.00
W	3.00	2.00	1.20	0.50	0.50	1.00	1.00	1.00
Y	39.00	33.50	15.10	30.10	29.40	22.10	22.30	21.20
Yb	3.60	3.20	1.46	3.07	2.96	1.85	1.77	1.71
Zr	214.00	204.00	125.10	85.00	198.10	124.00	126.00	115.00

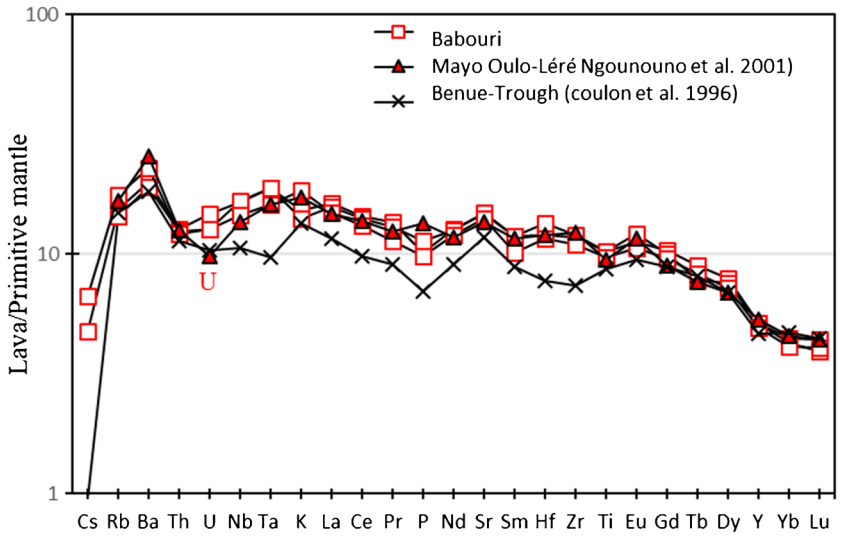

Fig. 10 Multi-element spectrum of Babouri basaltic flows normalized to the early mantle of McDonough and Sun (1995), compared to those of Mayo Oulo-Lere (Ngounouno et al. 2001) and Benue Trough (Coulon et al. 1996)

Table 3 Rare earth elements in sedimentary and volcanic rocks of Mayo Mbota

	S1M3	S2M2	S1M4	S2M1	S3M5	S1Vol1	S1Vol2	S2Vol3
La	56.10	50.50	16.90	28.90	17.70	10.00	9.70	9.20
Ce	117.50	102.50	30.80	62.50	38.40	23.20	22.50	21.20
Pr	13.55	11.80	3.40	14.47	4.48	3.30	3.15	2.76
Sm	10.50	9.04	2.58	5.24	3.99	4.59	4.62	3.95
Eu	1.98	1.78	0.77	1.22	1.20	1.64	1.77	1.55
Gd	8.94	7.92	2.93	5.27	4.85	5.31	5.17	4.90
Tb	1.30	1.15	0.43	0.85	0.79	0.84	0.74	0.78
Dy	7.69	6.85	2.76	5.17	5.15	5.03	4.83	4.60
Ho	1.33	1.15	0.57	1.07	1.14	0.80	0.86	0.80
Er	4.21	3.58	1.68	3.33	3.36	2.45	2.64	2.20
Tm	0.57	0.48	0.24	0.50	0.41	0.25	0.28	0.25
Yb	3.60	3.20	1.46	3.07	2,96	1.85	1.77	1.71
Lu	0.47	0.46	0.23	0.45	0,47	0.28	0.25	0.26
ΣREE	227.74	200.41	64.75	132.04	84.90	59.54	58.28	54.16
LREE	199.63	175.62	54.45	112.33	65.77	42.73	41.74	38.66
HREE	28.11	24.79	10.30	19.71	19.13	16.81	16.54	15.50
LREE/HREE	7.10	7.08	5.28	5.69	3.43	2.54	2.52	2.49
(La/Yb)N	1.50	1.52	1.12	0.91	0.57	3.64	3.69	3.63

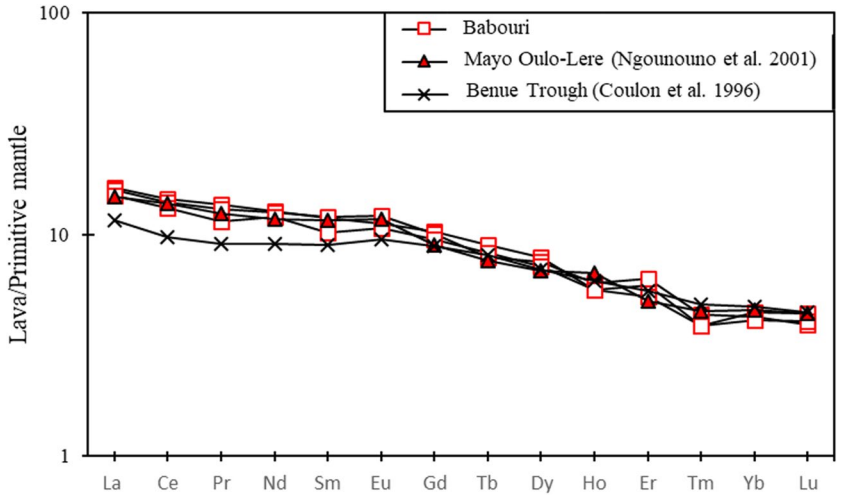

Fig. 11 Rare earth spectrum of Babouri basaltic flows normalized to the early mantle of McDonough and Sun (1995), compared to those of Mayo Oulo-Lere (Ngounouno et al. 2001) and Benue Trough (Coulon et al. 1996)

variations in the basaltic lava flows. These flows are responsible for both low metamorphism, resulting in a schistose appearance in marls, and high metamorphism, causing calcination in marls (Balla 2017) with a friable aspect found in the Mayo Mbota. The interaction between basaltic flows and schistose marls suggests possible lava contamination through the assimilation of marls at the contact point.

Sedimentology in the Mayo Mbota consists of coarse sandstones at the base, medium sandstones, fine sandstones, and shistone marls. Mechano-chemical contacts in this basin occur due to pressure dissolution (Bjorlykke et al. 1989), with selective dissolution at contact points of particles under significant stress. Pisolithic to oolitic textures in marls, rich in quartz, suggest a granitic and gneissic source (Dickinson 1985). Mineralogically, marls are composed of calcite, feldspar, quartz, kaolinite, illite, smectite, analcime, anatase, and muscovite.

The Babouri basalts exhibit microlitic porphyry and dolerite textures with microlites and microphenocrysts of plagioclase, clinopyroxene, olivine crystals, amphibole phenocrysts, and oxide crystals—typical features of oceanic tholeiites. The preferential orientation of crystals suggests transportation in a still-fluid magma prior to solidification (Mackenzie and Adams 1995).

These basalts have the composition of andesitic basalts and are located in the domain of oceanic-type tholeiites. They characterize a geodynamic context of rift opening linked to the Atlantic Ocean, hence the parallelism of the spectra between

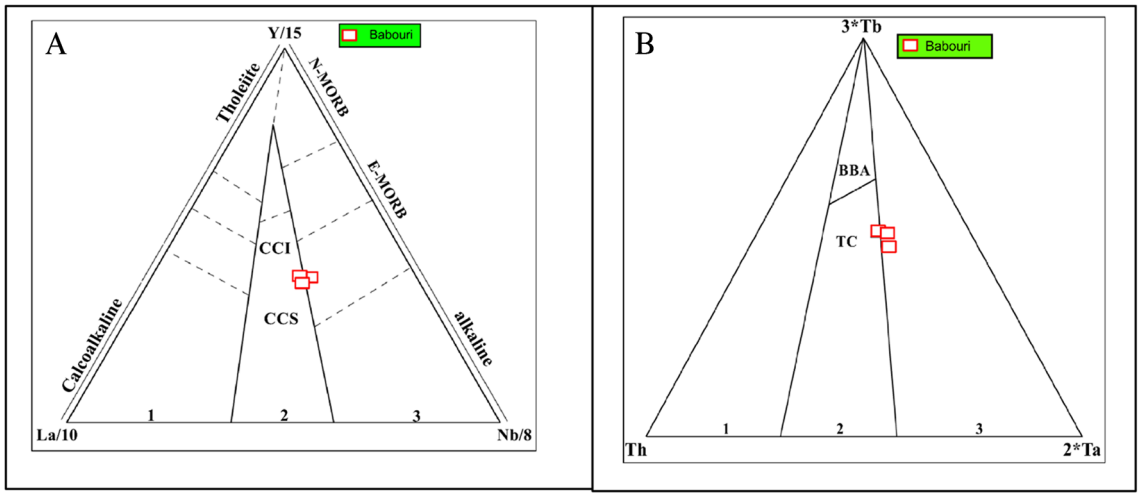

Fig. 12 Geodynamic context of basalts: **A** emplacement domain of the studied lavas according to Cabanis and Lecolle (1988). LCC, lower continental crust; UCC, upper continental crust; 1, orogenic domain (compressive); 2, late to post-orogenic intracontinental domain (compressive to distensive); 3, non-orogenic domain (distensive). **B** Triangular diagram Th-Tbx3-Tax2 of Cabanis and Thiéblemont (1989) highlighting the emplacement sites of Babouri's lavas. 1, orogenic arc domain; 2, continental tholeiites (CT) and basalts of the back basins (BBA) domain; 3, anorogenic domain of ridge tholeiites and intraplate alkaline basalts

the lavas studied, which are compared with those of the Benue rift in Nigeria (Coulon et al. 1996) and those of the Mayo Oulo basin (Ngounouno et al. 2001). The negative Th and U anomalies observed in the trace element spectra of these tholeiites certainly reflect their contamination either by the continental crust or by terrigenous sediments. This hypothesis could be reflected in the approximation of these elements (Fig. 17). The low values of the (La/Yb)N ratio of the Babouri tholeiites (≈3.6), like those of Benue Trough and Mayo Oulo, imply a high partial melting rate of the source mantle. This would explain the horizontal trends in the multi-element spectra. These rocks would come from a mantle that is not completely depleted. This is justified by their position in the E-MORB field of Wood's diagram (Wood 1980) (Fig. 18).

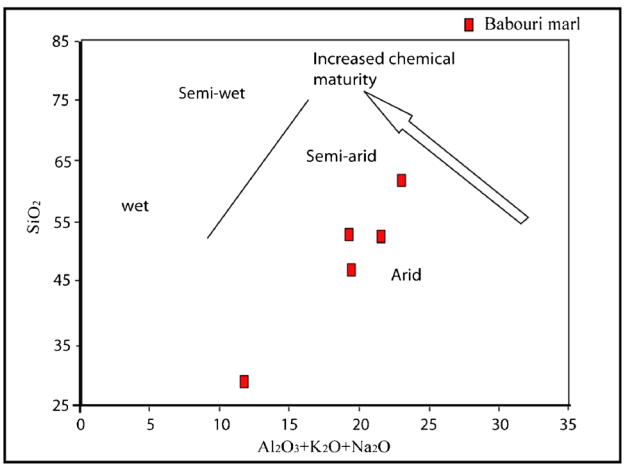

Fig. 13 SiO_2 vs. (Al_2O_3 + K_2O + Na_2O) diagram showing the depositional environment and chemical maturity level of the Babouri marl sediments after Suttner and Dutta (1986)

The Babouri marls were fed by the erosion products of felsic rocks, indicated by the K_2O versus Rb diagram (Floyd et al. 1990). The various Th/U, Zr/Y, and Hf/Ta ratios greater than 1 (Bhushan and Priyadarshi 2010) and the high Al_2O_3/TiO_2 ratio (Fiffe and Pickerill 1993) support the hypothesis of a terrigenous detrital input dominated by felsic rocks. The SiO_2/Al_2O_3 ratios of the marls are moderate with values between 3.12 and 4.12%, indicating a low to moderate degree of chemical maturity, according to the maturity limits proposed by Asiedu et al. (2004), confirmed by the SiO_2 versus Al_2O_3 + K_2O + Na_2O diagram of Suttner and Dutta (1986). The positive correlation of TiO_2 and Al_2O_3 implies an accumulation of immobile elements Nb and Ba which, coupled with the lower CIA, indicates moderate chemical alteration of terrigenous detrital materials (Young and Nesbitt 1998). The variable LREE/HREE and (La/Yb)N ratios (Table 3) may suggest an effect of heterogeneous sorting of heavy minerals with variable enrichment of dense and resistant minerals (Kasanzu et al. 2008; Nyobe et al. 2018). The variable LREE/HREE and (La/Yb)N ratios are related to the variable nature of REE mineral carriers. In fact, low LREE/HREE ratios lead to low (La/Yb)N ratios (Li et al. 2005).

Conclusion

The investigation conducted in the Mayo Mbota area involved a thorough examination of identified outcrops, resulting in the identification of four distinct lithological

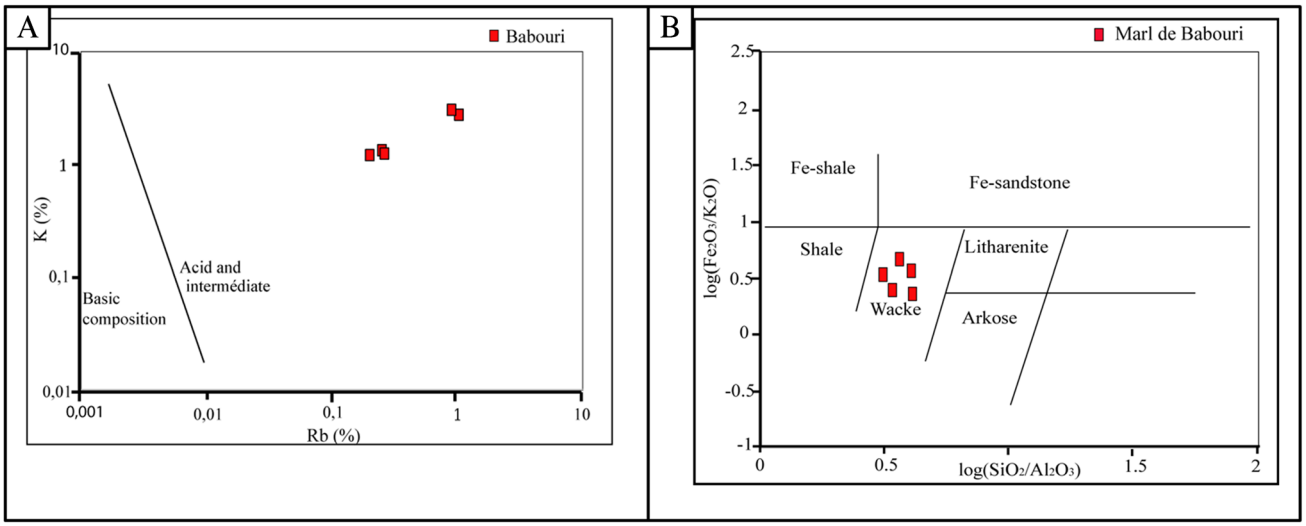

Fig. 14 The source of the marls: **A** fragmentation of K as a function of Rb (Floyd et al. 1990), **B** geochemical classification of samples according to the log (Fe_2O_3/K_2O) versus log (SiO_2/Al_2O_3) diagram (Herron 1988)

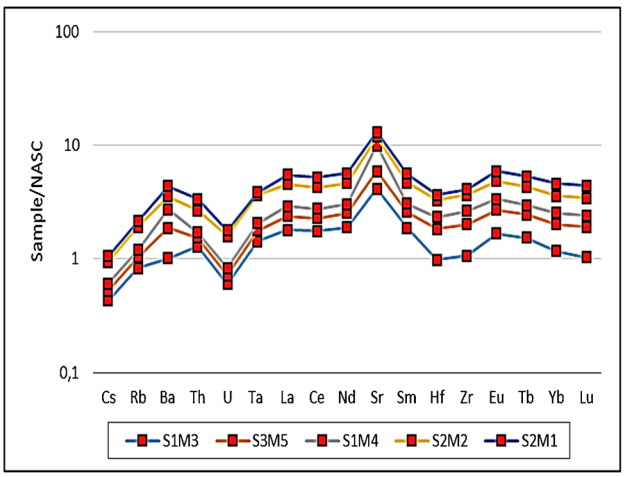

Fig. 15 Multi-element spectra of Babouri marls normalized to the NASC (Gromet et al. 1984)

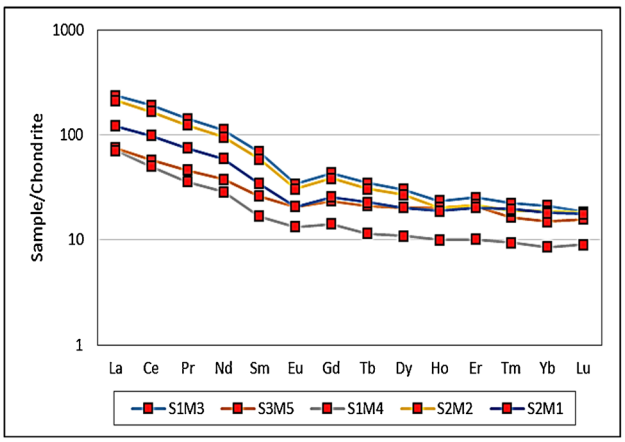

Fig. 16 Rare earth spectrum of Baburi's marls normalized to chondrite

facies: coarse sandstone, medium sandstone, fine sandstone, and shale marl. The volcanic flows were determined to be post-sedimentary in nature. Petrographic analysis of the sedimentary rocks revealed quartz as the predominant element. On the other hand, volcanic rocks exhibited two distinct textures: a microlitic porphyritic texture containing oxides, plagioclase phenocrysts, and clinopyroxenes and a doleritic porphyritic texture characterized by automorphic phenocrysts of plagioclase, clinopyroxenes, oxide crystals, olivines, and amphibole mineral phenocrysts.

The mineralogical composition of marls encompassed primary minerals like calcite, feldspar, quartz, and muscovite, alongside secondary minerals such as kaolinite, illite, and smectite. Titanium oxides (anatase) and hydrated sodium silicates (analcime) were also identified. Geochemical analyses indicated that the Babouri basalts fall within the category of oceanic tholeiites, displaying an andesitic basalt composition and being emplaced in an orogenic (distensive) setting. The geochemistry of the Cretaceous sediments in Mayo Mbota classified them as intermediate to acidic rocks of active continental margins, deposited in an arid to semi-arid environment. These sediments were formed through the accumulation of alteration products derived from felsic rocks, specifically granite and/or gneiss.

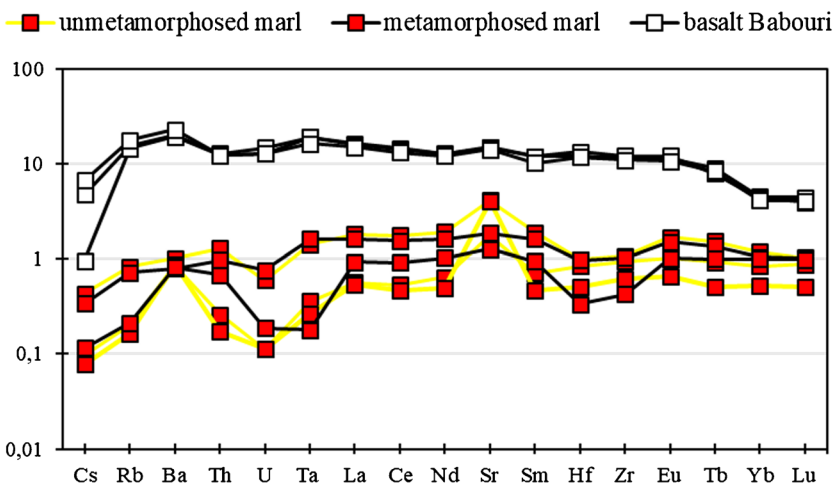

Fig. 17 Evidence of selective metamorphism with elements such as Th, U, and Sr

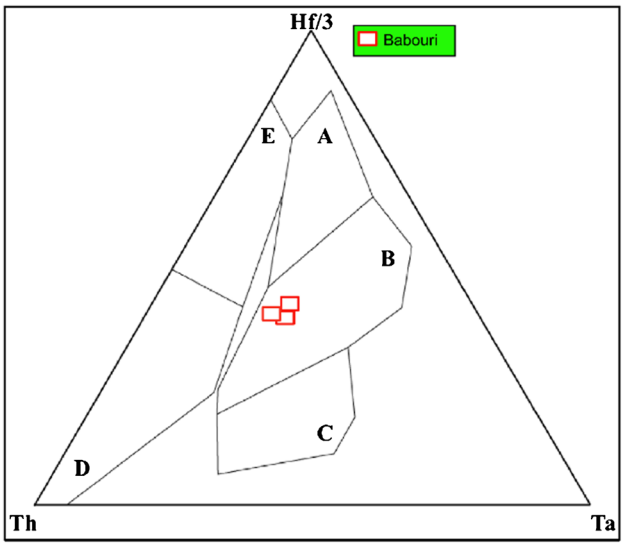

Fig. 18 Wood's (1980) Hf/3-Th-Ta diagram for the Babouri lavas. A, N-MORB; B, E-MORB; C, alkaline domain; D, Hf > 3.0 volcanic arc basalts; and E, calc-alkaline basalt domain with Hf/Th > 3.0

Author contribution Not applicable.

Availability of code Not applicable.

Data Availability Not applicable.

Declarations

Conflict of interest The authors declare no competing interests.

References

Almeida FF, Hasui Y, Brito de Neves BB, Fuck RA (1981) Brazilian structural provinces. Earth Sci Rev 17:1–29

Asiedu DK, Dampare SB, Asmoah SP, Banoeng-Yacubo B, Ossae S, Nyarko BJB, Manu J (2004) Geochemistry of paleoprotorozoic metasedimentary rocks from the Birim diamontiferous field, southern Ghana: implications for provenance and crustal evolution at the Archean-Proterozoic boundary. Geochem J 38:215–228

Balla OAD (2017) Lithostratigraphie, sédimentologie, analyse séquentielle et paléogéographique du Bassin crétacé de Babouri-Figuil. Thèse Université de Yaoundé I:177p

Balla OAD, Abolo AN, Edjengte DEP, Mohamed A, Ekoa BAZ (2022) Tectono-sedimentary framework of the Cretaceous intracontinental Babouri-Figuil basin (Benue Trough, North-Cameroon). Arab J Geosci 15(1):66. https://doi.org/10.1007/s12517-021-09367-3

Bhushan S, Priyadarshi S (2010) Geochemistry of clastic sediments from Sargur supracrustals and Bababudan group, Karnataka: implications on Archean Proterozoic boundary. J Geol Soci Ind 75:829–840https://doi.org/10.1007/s12517-024-11916-5

Bjorlykke K, Ramm M, Saigal GC (1989) Sandstone diagenesis and porosity modification during basin evolution. Geologische Rundschau 78(1):243–268

Brito de Neves BD, Schmus V, Fetter A (2001) North-West Africa North-Eastern Brazil. Major tectonic links and correlation problems. J Afr Earth Sci 34:275–273

Cabanis B, Lecolle M (1988) Le diagramme La/10—Y/15—Nb/8 : un outil pour la discrimination des séries volcaniques et la mise en évidence des processus de mélange et/ou de Contamination crustale. C R Acad Sci Paris 309(2):2023–2029

Cabanis B, Thiéblemont D (1989) La discrimination des tholéiites continentales et des basaltes arrière-arc. Proposition d'un nouveau diagramme Th–Tbx3–Tax2. Bull Soc Géol France 4(6):927–935

Castaing C, Triboulet C, Feybesse J, Chévremont P (1993) Tectono-métamorphic evolution of Ghana, Togo, Benin in the light of the PanAfrican/Braziliano orogeny. Tectonophysics 218:323–347

Coulon C, Vidal P, Dupuy C, Baudin P, Popoff M, Maluski H, Hermitte D (1996) The Mesozoic to Early Cenozoic magmatism of the Benue rough (Nigeria); geochemical evidence for the involvement of the St Helena plume. J Petrol 37(6):1341–1358

Davidson and Reginaldo (1989) Tectonic evolution for the seripano Fold Belt, NE Brazil, during the Braziliano Orogeny. PrecambrianResearch 45:319–342

Dickinson W (1985) Interpreting provenance relations from detrital modes of sandstones. In: Zuffa GG (ed) Provenance of Arenites, NATO-ASI Series, vol 148. Reidel Publishing Company, pp 333–361

Fiffe L, Pickerill R (1993) Geochemistry of Upper Cambrian-Lower Ordovician black shale along a northeastern Appalachian transect. Geol Soc Am Bull 105:897910

Floyd P, Franke W, Shail R, Dorr W (1990) Provenance and depositional environment of thenohercynian synorogenic grewacke from the Giessen nappe, Germany. Geologische Rundschau 79:611–626

Gromet LP, Dymek RF, Haskin LA, Korotev RL (1984) The "North American shale composite" : its compilation, major and trace element characteristics, vol 48. Pergamon Press Ltd. 1984. Printed in U.S.A. Geochumco n Cosmoch~mrco Ada, pp 2469–2482

Herron M (1988) Geochimical classification of terrigenous sands and shales from core log data. J Sediment Petrol 58:820–829

Kasanzu C, Mah M, Manya S (2008) Geochemistry of finegrained clastic sedimentary rocks of the Neoproterozoic Ikorongo group, NE Tanzania: implications for provenance and source rock weathering. Precambrian Res 164:201–213

Le Maître RW (2002) Igneous rocks. A classification and glossary ofterms. In: Recommendations of the International Union of Geological Sciences Subcommission on the systematics of Igneous-Rocks. Cambridge University Press, Cambridge

Li Q, Liu S, Han B, Zhang J, Chu Z (2005) Geochemistry of metasedimentary rocks of the Proterozoic Xingxingxia complex: implications for provenance and tectonic setting of the eastern segment of the central Tianshan tectonic zone, northwestern China. J Afr Earth Sci 42:287–306

Ma JL, Wei GJ, Xu YG, Long WG, Sun WD (2007) Mobilization and re-distribution of major and trace elements during extreme weathering of basalt in Hainan Island, South China. Geochim Cosmochim Acta 71:3223–3237

Mackenzie WS, Adams AE (1995) Atlas d'initiation à la pétrographie. Masson, Paris, p 180

Maurin JC, Guiraud R (1990) Relationships between Tectonics and Sedimentation in the Barremo-Aptian Intracontinental Basins of Northern Cameroon. J Afr Earth Sci 10:331-340. https://doi.org/10.1016/0899-5362(90)90064-L

McDonough WF, Sun SS (1995) The composition of the Earth. chem. Geol. 120:223 253

Miyashiro A (1974) Volcanic rock series in island arcs and active continental margins. Am J Sci 274(4):321–355

Ngako V (1999) Les Déformations Continentales Panafricaines en Afrique Centrale : Résultat d'un Poinconnement de Type Himalayen. Thèse de Doctorat d'Etat,. University of Yaoundé I, Yaoundé, p 301

Ngnotué T, Nzenti JP, Barbey P, Tchoua FM (2000) The Ntui Bétamba high gradegneisses: a northward extension of the pan-African Yaoundé gneisses in Cameroon. J Afr Earth Sci 31:369–381

Ngounouno I, Déruelle B, Guiraud R, Vicat JP (2001) Magmatismes tholéiitique et alcalin des demigrabens crétacés de Mayo Oulo-Léré et de Babouri-Figuil (Nord du Cameroun-Sud du Tchad) en domaine d'extension continentale. Compt Rend Acad Sci-Ser IIA-Earth Planet Sci 333(4):201–207

Njel U0 (1988) Contribution à l'étude de l'orogène pan-africain : la ceinture volcano-sédimentaire de Poli (Nord-Cameroun) : paléogéographie, géochimie, minéralisations cuprifères associées. These Doctorat de l'I.N.P.L. 220p

Nyobe JM, Sababa E, Bayiga EC, Ndjigui PD (2018) Mineralogical andgeochemical features of alluvial sediments from the Lobo watershed (Southern Cameroon): implications for rutile exploration. C.R. Geoscience 350:119–129

Nzenti JP, Abaga B, Suh CE, Nzolang C (2011) Petrogenesis of peraluminous magmas from the Akum-Bamenda Massif, Pan-African fold belt, Cameroon. Int Geol Rev 53(10):1121–1149

Nzenti JP, Barbey P, Bertrand JM, Macaudière J (1994) La Chaîne Panafricaine au Cameroun: Cherchons suture et modèle!, 15ème Réunion des Sciences de la Terre. Société Géologique de France, Nancy, France, p 99

Nzenti JP, Ngako V, Kambou R, Penaye J, Bassahak J, Njel OU (1992) Structures Régionales de la Chaine Panafricaine du Nord-Cameroun. Comptes Rendus de L'académie des Sci, Paris 315(2):209–215

Nzenti JP, Njanko T, Njiosseu ELT, Tchoua FM (1998) Les domaines granulitiques de la chaine panafricaine Nord-Equatoriale au Cameroun. In: Vicat, J.P., Bilong, P., (Eds.), Geologie et environnement au Cameroun, GEOCAM 1, 255–264

Pearce JA (1975) Basalt geochemistry used to investigage past tectonic environment on Cyprus. Tectonophysics 25:41–68

Pourmand A, Dauphas N, Ireland TJ (2012) A novel extraction chromatography and MC-ICP-MS technique for rapid analysis of REE, Sc and Y: revising CI-chondrite and Post-Archean Australian Shale (PAAS) abundances. Chem Geol 291:38–54

Schwoerer P (1965) Notice explicative sur la feuille de Garoua-Est. Carte géologique de reconnaissance au 1/500,000. Direction des Mines et de la Géologie 49

Sibuet JC, Mascle J (1978) Plate kinetic implications of Atlantic equatorial fracture zones trends. J Geophys Res 83:3401–3421

Suttner L, Dutta P (1986) Alluvial sandstone composition and paleoclimate, I Framework mineralogy. J Sediment Petrol 56(3):329–345

Tanko Njiosseu EL, Nzenti JP, Njanko T, Kapajika B, Nedelec A (2005) New U/Pb zircon âges from Tonga (Cameroon): coexisting Eburnean Transamazonian (2.1 Ga) and Pan-African (0.6 Ga) impreints. Compte Rendu Géosciences 337:551–562

Toteu SF, Bertrand JML, Penaye J, Macaudiere J, Angoua S, Barbey P (1990) Cameroon: a tectonic keystone in the Pan-African network. In: Lewry JF, Stauffer MR (eds) The Early Proterozoic Trans-Hudson Orogen of North America, vol 37. Geological Association of Canada Special Paper, pp 483–496

Toteu SF, Michard A, Bertrand JM, Rocci G (1987) U/Pb dating of Precambrian rocks from northern Cameroon, orogenic evolution and chronology of the Pan-African belt of central Africa. Precambrian Res 37:71–87

Toteu SF, Penaye J, Poudjomdjomani YH (2004) Geodynamic evolution of the Pan-African belt in central Africa with special reference to Cameroon. Can J Earth Sci 41:73–85

Wood DA (1980) The application of the Th–Hf–Ta diagram to problems of tectonomagmatic classification and to establishing the nature of crustal contamination of basaltic lava of the British Tertiary volcanic province. Earth Planet Sci Lett 50:11–30

Young G, Nesbitt H (1998) Process controlling the distribution of Ti and Al in weathering profiles, siliclastic sediments and sedimentary rocks. J Sed Res 68:448

Yusoff ZM, Ngwenya BT, Parsons I (2013) Mobility and fractionation of REEs during deep weathering of geochemically contrasting granites in a tropical setting, Malaysia. Chem Geol 349:71–86